THE UNIVERSITY of EDINBURGH

Edinburgh Research Explorer

Left/right asymmetry in Dyakonov–Tamm-wave propagation guided by a topological insulator and a structurally chiral material

Citation for published version:
Chiadini, F, Fiumara, V, Mackay, TG, Scaglione, A & Lakhtakia, A 2016, 'Left/right asymmetry in Dyakonov–Tamm-wave propagation guided by a topological insulator and a structurally chiral material', *Journal of optics*, vol. 18, no. 11, 115101. https://doi.org/10.1088/2040-8978/18/11/115101

Digital Object Identifier (DOI):
10.1088/2040-8978/18/11/115101

Link:
Link to publication record in Edinburgh Research Explorer

Document Version:
Publisher's PDF, also known as Version of record

Published In:
Journal of optics

General rights
Copyright for the publications made accessible via the Edinburgh Research Explorer is retained by the author(s) and / or other copyright owners and it is a condition of accessing these publications that users recognise and abide by the legal requirements associated with these rights.

Take down policy
The University of Edinburgh has made every reasonable effort to ensure that Edinburgh Research Explorer content complies with UK legislation. If you believe that the public display of this file breaches copyright please contact openaccess@ed.ac.uk providing details, and we will remove access to the work immediately and investigate your claim.

Download date: 06. May. 2023

IOPscience iopscience.iop.org

Home Search Collections Journals About Contact us My IOPscience

Left/right asymmetry in Dyakonov–Tamm-wave propagation guided by a topological insulator and a structurally chiral material

This content has been downloaded from IOPscience. Please scroll down to see the full text.

2016 J. Opt. 18 115101

(http://iopscience.iop.org/2040-8986/18/11/115101)

View the table of contents for this issue, or go to the journal homepage for more

Download details:

IP Address: 129.215.240.223
This content was downloaded on 27/10/2016 at 12:39

Please note that terms and conditions apply.

You may also be interested in:

Theory of Dyakonov–Tamm waves at the planar interface of a sculptured nematic thin filmand an isotropic dielectric material
Kartiek Agarwal, John A Polo Jr and Akhlesh Lakhtakia

Rugate-filter-guided propagation of multiple Fano waves
Muhammad Faryad, Husnul Maab and Akhlesh Lakhtakia

On the propagation of Voigt waves in energetically active materials
Tom G Mackay and Akhlesh Lakhtakia

Surface plasmon–polariton wave propagation guided by a metal slab in a sculpturednematic thin film
Muhammad Faryad and Akhlesh Lakhtakia

Counterposition and negative phase velocity in uniformly moving dissipative materials
Tom G Mackay and Akhlesh Lakhtakia

On the propensity of guiding surface-plasmon-polariton waves by the back-contact of an amorphous silicon p-i-n solar cell
Mahmoud R M Atalla and Samia A Suliman

OPEN ACCESS
IOP Publishing
Journal of Optics
J. Opt. 18 (2016) 115101 (9pp)
doi:10.1088/2040-8978/18/11/115101

Left/right asymmetry in Dyakonov–Tamm-wave propagation guided by a topological insulator and a structurally chiral material

Francesco Chiadini[1], Vincenzo Fiumara[2], Tom G Mackay[3,4], Antonio Scaglione[1] and Akhlesh Lakhtakia[4]

[1] Department of Industrial Engineering, University of Salerno, via Giovanni Paolo II, 132—Fisciano (SA), I-84084, Italy
[2] School of Engineering, University of Basilicata, Viale dell'Ateneo Lucano 10, I-85100 Potenza, Italy
[3] School of Mathematics and Maxwell Institute for Mathematical Sciences, University of Edinburgh, Edinburgh EH9 3FD, UK
[4] Department of Engineering Science and Mechanics, Pennsylvania State University, University Park, PA 16802–6812, USA

E-mail: akhlesh@psu.edu

Received 23 June 2016, revised 25 August 2016
Accepted for publication 26 August 2016
Published 23 September 2016

Abstract

The propagation of Dyakonov–Tamm waves guided by the planar interface of an isotropic topological insulator and a structurally chiral material, both assumed to be nonmagnetic, was investigated by numerically solving the associated canonical boundary-value problem. The topologically insulating surface states of the topological insulator were quantitated via a surface admittance γ_{TI}, which significantly affects the phase speeds and the spatial profiles of the Dyakonov–Tamm waves. Most significantly, it is possible that a Dyakonov–Tamm wave propagates co-parallel to a vector $\mathbf{u}$ in the interface plane, but no Dyakonov–Tamm wave propagates anti-parallel to $\mathbf{u}$. The left/right asymmetry, which vanishes for $\gamma_{TI} = 0$, is highly attractive for one-way on-chip optical communication.

Keywords: chiral smectic liquid crystal, Dyakonov–Tamm wave, one-way device, sculptured thin film, structurally chiral material, topological insulator

(Some figures may appear in colour only in the online journal)

1. Introduction

Dyakonov–Tamm waves are electromagnetic surface waves whose propagation is guided by the planar interface of two dielectric materials, one of which is isotropic and homogeneous whereas the second is anisotropic and periodically nonhomogeneous normal to the interface plane [1]. In contrast, the second partnering material must be isotropic for Tamm-wave propagation [2–5], whereas that material must be homogeneous for Dyakonov-wave propagation [6–8]. All three types of surface waves propagate ideally without attenuation, unlike surface-plasmon-polariton waves [9], as all three exist in all-dielectric metamaterial architectures [10]. Dyakonov and Dyakonov–Tamm waves offer different phase speeds in different directions of propagation in the interface plane, which makes them more attractive than Tamm waves for communication. But, while the allowed directions of propagation of Dyakonov waves are confined to two minute angular sectors (typically, each less than 1° in width [8, 11]) in the interface plane, Dyakonov–Tamm waves were theoretically predicted not to suffer from that restriction. The existence of these waves has been confirmed recently in two distinct experimental configurations [12, 13].

Original content from this work may be used under the terms of the Creative Commons Attribution 3.0 licence. Any further distribution of this work must maintain attribution to the author(s) and the title of the work, journal citation and DOI.

 © 2016 IOP Publishing Ltd Printed in the UK

Theoretical investigation [14] has recently shown that left/right asymmetry can be introduced in Dyakonov-wave propagation by

(i) endowing the isotropic, homogeneous, dielectric partnering material with topologically insulating surface states (TISS) [15–17] and
(ii) choosing the anisotropic, homogeneous, dielectric partnering material to possess orthorhombic crystallographic symmetry such that no more than one of the three eigenvectors of its relative permittivity dyadic lies in the interface plane.

Then, the Dyakonov wave propagating coparallel to a vector **u** in the interface plane has a different phase speed and different spatial profile as compared to the Dyakonov wave which propagates antiparallel to **u**. Indeed, it may be possible for a Dyakonov wave to propagate coparallel to **u** but for no Dyakonov to propagate antiparallel to **u**. We refer to this asymmetry with respect to interchanging the direction of surface-wave propagation as left/right asymmetry. The exploitation of left/right asymmetry is promising for one-way optical devices, which could reduce backscattering noise [18] in optical communication networks, microscopy, and tomography, for example. Let us note here that left/right asymmetry is not exhibited when the TISS are replaced by ordinary surface conducting states [19, 20].

Although the incorporation of an isotropic topological insulator (TI) as a partnering material [16, 21] introduces left/right asymmetry in surface-wave propagation, the angular sectors of allowable propagation remain minute in extent [14]. With the aim of widening those angular sectors, we decided to make the anisotropic partnering material periodically nonhomogeneous in the direction normal to the interface plane. Specifically, we chose that partnering material to be a structurally chiral material (SCM) [1]—exemplified by chiral smectic liquid crystals [22] and chiral sculptured thin films [23]—the other partnering material being an isotropic TI [24, 25].

The plan of this paper is as follows. Section 2 contains a formulation of the canonical problem for Dyakonov–Tamm-wave propagation guided by the planar interface of an isotropic TI and an SCM. In the canonical problem, all space is partitioned into two half spaces, one of which is occupied by one partnering material and the second by the other partnering material. Although practically unimplementable in the strict sense, the canonical problem lies at the heart of practically implementable configurations such as the prism-coupled, grating-coupled, and waveguide-coupled configurations [26, 27]. Numerical results are provided and discussed in section 3.

An $\exp(-\mathrm{i}\omega t)$ dependence on time t is implicit, with ω denoting the angular frequency and $\mathrm{i} = \sqrt{-1}$. The free-space wavenumber, the free-space wavelength, and the intrinsic impedance of free space are denoted by $k_0 = \omega\sqrt{\varepsilon_0\mu_0}$, $\lambda_0 = 2\pi/k_0$, and $\eta_0 = \sqrt{\mu_0/\varepsilon_0}$, respectively, with ε_0 and μ_0 being the permeability and permittivity of free space. The speed of light in free space is denoted by $c_0 = 1/\sqrt{\varepsilon_0\mu_0}$.

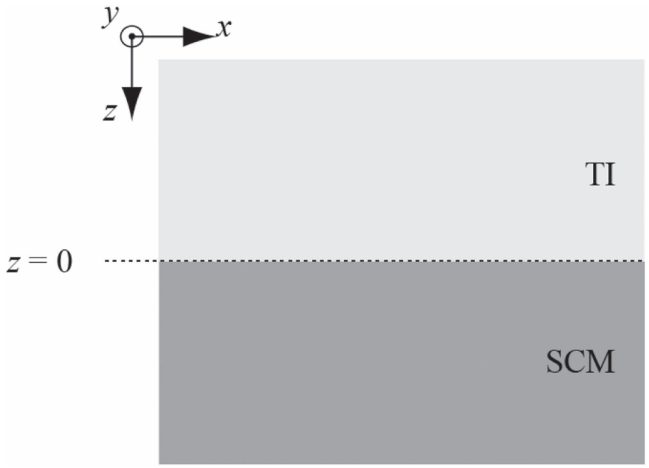

Figure 1. Schematic of the boundary-value problem solved.

Vectors are in boldface; dyadics are underlined twice; Cartesian unit vectors are identified as $\hat{\mathbf{u}}_x$, $\hat{\mathbf{u}}_y$, and $\hat{\mathbf{u}}_z$; column vectors are in boldface and enclosed with square brackets; and matrixes are underlined twice and enclosed with square brackets.

2. Theory

A schematic of the boundary-value problem for the propagation of the Dyakonov–Tamm wave is provided in figure 1. The half-space $z < 0$ is occupied by an isotropic TI with a relative permittivity $\varepsilon_{\mathrm{TI}} = n_{\mathrm{TI}}^2$ and a surface admittance γ_{TI} which quantifies the TISS [16] that arise in consequence of a geometric phase that cannot be gauged away in a cyclic system [28, 29]. Alternatively, the half-space $z < 0$ can be modeled as being occupied by an isotropic, nonreciprocal, achiral, nonmagnetic material with relative permittivity $\varepsilon_{\mathrm{TI}}$ and Tellegen parameter γ_{TI}; but we prefer the former description because it brings out the presence of TISS very clearly [20] and conforms to the Post constraint [21].

The half-space $z > 0$ is occupied by an SCM whose permittivity dyadic is given by

$$\underline{\underline{\varepsilon}}_{\mathrm{SCM}}(z) = \varepsilon_0\, \underline{\underline{S}}_z(z) \cdot \underline{\underline{S}}_y(\chi) \cdot \underline{\underline{\varepsilon}}^{\circ}_{\mathrm{ref}} \cdot \underline{\underline{S}}_y^{-1}(\chi) \cdot \underline{\underline{S}}_z^{-1}(z). \quad (1)$$

Here, the dyadics

$$\left.\begin{aligned} \underline{\underline{S}}_z(z) &= (\hat{\mathbf{u}}_x\hat{\mathbf{u}}_x + \hat{\mathbf{u}}_y\hat{\mathbf{u}}_y)\cos(\pi z/\Omega) \\ &\quad + h\,(\hat{\mathbf{u}}_y\hat{\mathbf{u}}_x - \hat{\mathbf{u}}_x\hat{\mathbf{u}}_y)\sin(\pi z/\Omega) + \hat{\mathbf{u}}_z\hat{\mathbf{u}}_z \\ \underline{\underline{S}}_y(\chi) &= (\hat{\mathbf{u}}_x\hat{\mathbf{u}}_x + \hat{\mathbf{u}}_z\hat{\mathbf{u}}_z)\cos\chi \\ &\quad + (\hat{\mathbf{u}}_z\hat{\mathbf{u}}_x - \hat{\mathbf{u}}_x\hat{\mathbf{u}}_z)\sin\chi + \hat{\mathbf{u}}_y\hat{\mathbf{u}}_y \\ \underline{\underline{\varepsilon}}^{\circ}_{\mathrm{ref}} &= \varepsilon_a\,\hat{\mathbf{u}}_z\hat{\mathbf{u}}_z + \varepsilon_b\,\hat{\mathbf{u}}_x\hat{\mathbf{u}}_x + \varepsilon_c\,\hat{\mathbf{u}}_y\hat{\mathbf{u}}_y \end{aligned}\right\}; \quad (2)$$

$h = 1$ for structural right-handedness and $h = -1$ for structural left-handedness; 2Ω is the structural period of the SCM along the z axis; and $\chi \in (0, \pi/2]$. Whereas $\varepsilon_a = \varepsilon_c \neq \varepsilon_b$ and $\chi = 0$ for cholesteric liquid crystals,

$\varepsilon_a \neq \varepsilon_b \neq \varepsilon_c$ and $\chi \in (0, \pi/2]$ for chiral smectic liquid crystals [22] and chiral sculptured thin films [23]. Both partnering materials are assumed to be nonmagnetic.

The field representation in the region $z > 0$ requires the formulation of the column vector [23, 27]

$$[\mathbf{f}(z)] = [e_x(z) \quad e_y(z) \quad h_x(z) \quad h_y(z)]^T \tag{6}$$

$$\begin{aligned}[\underline{\underline{P}}(\zeta, \psi)] = \omega &\begin{bmatrix} 0 & 0 & 0 & \mu_0 \\ 0 & 0 & -\mu_0 & 0 \\ \varepsilon_0(\varepsilon_c - \varepsilon_d)\cos\zeta\,\sin\zeta & -\varepsilon_0(\varepsilon_c\cos^2\zeta + \varepsilon_d\sin^2\zeta) & 0 & 0 \\ \varepsilon_0(\varepsilon_c\sin^2\zeta + \varepsilon_d\cos^2\zeta) & -\varepsilon_0(\varepsilon_c - \varepsilon_d)\cos\zeta\,\sin\zeta & 0 & 0 \end{bmatrix} + q\,\frac{\varepsilon_d(\varepsilon_a - \varepsilon_b)}{\varepsilon_a\,\varepsilon_b}\sin\chi\cos\chi \\ &\times \begin{bmatrix} \cos\zeta\cos\psi & \sin\zeta\cos\psi & 0 & 0 \\ \cos\zeta\sin\psi & \sin\zeta\sin\psi & 0 & 0 \\ 0 & 0 & \sin\zeta\sin\psi & -\sin\zeta\cos\psi \\ 0 & 0 & -\cos\zeta\sin\psi & \cos\zeta\cos\psi \end{bmatrix} + \frac{q^2}{\omega\varepsilon_0}\,\frac{\varepsilon_d}{\varepsilon_a\,\varepsilon_b}\begin{bmatrix} 0 & 0 & \cos\psi\sin\psi & -\cos^2\psi \\ 0 & 0 & \sin^2\psi & -\cos\psi\sin\psi \\ 0 & 0 & 0 & 0 \\ 0 & 0 & 0 & 0 \end{bmatrix} \\ &+ \frac{q^2}{\omega\mu_0}\begin{bmatrix} 0 & 0 & 0 & 0 \\ 0 & 0 & 0 & 0 \\ -\cos\psi\sin\psi & \cos^2\psi & 0 & 0 \\ -\sin^2\psi & \cos\psi\sin\psi & 0 & 0 \end{bmatrix} \end{aligned} \tag{8}$$

2.1. Field representations

We consider the Dyakonov–Tamm wave to be propagating parallel to the unit vector $\hat{\mathbf{u}}_{\text{prop}} = \hat{\mathbf{u}}_x\cos\psi + \hat{\mathbf{u}}_y\sin\psi$, $\psi \in [0°, 360°)$, in the xy plane and decaying far away from the interface $z = 0$. With q as the wavenumber of the Dyakonov–Tamm wave, the electric and magnetic phasors can be represented everywhere by

$$\left.\begin{aligned}\mathbf{E}(\mathbf{r}) &= \mathbf{e}(z)\exp(\mathrm{i}q\hat{\mathbf{u}}_{\text{prop}}\cdot\mathbf{r}) \\ \mathbf{H}(\mathbf{r}) &= \mathbf{h}(z)\exp(\mathrm{i}q\hat{\mathbf{u}}_{\text{prop}}\cdot\mathbf{r})\end{aligned}\right\}. \tag{3}$$

In the region $z < 0$, the field phasors may be written as [21, 27]

$$\begin{aligned}\mathbf{e}(z) = [&A_1(-\hat{\mathbf{u}}_x\sin\psi + \hat{\mathbf{u}}_y\cos\psi) \\ &+ A_2\left(\frac{\alpha_{\text{TI}}}{k_0}\,\hat{\mathbf{u}}_{\text{prop}} + \frac{q}{k_0}\,\hat{\mathbf{u}}_z\right)] \\ &\times \exp(-\mathrm{i}\alpha_{\text{TI}}z), \quad z < 0\end{aligned} \tag{4}$$

and

$$\begin{aligned}\mathbf{h}(z) = \eta_0^{-1}&\left[A_1\left(\frac{\alpha_{\text{TI}}}{k_0}\,\hat{\mathbf{u}}_{\text{prop}} + \frac{q}{k_0}\,\hat{\mathbf{u}}_z\right)\right. \\ &\left. - A_2\,n_{\text{TI}}^2(-\hat{\mathbf{u}}_x\sin\psi + \hat{\mathbf{u}}_y\cos\psi)\right] \\ &\times \exp(-\mathrm{i}\alpha_{\text{TI}}z), \quad z < 0,\end{aligned} \tag{5}$$

where A_1 and A_2 are unknown scalars, q is positive and real-valued for unattenuated propagation in the xy plane, $q^2 + \alpha_{\text{TI}}^2 = k_0^2\varepsilon_{\text{TI}}$, and $\text{Im}(\alpha_{\text{TI}}) > 0$ for attenuation as $z \to -\infty$.

which satisfies the matrix differential equation [1]

$$\frac{\mathrm{d}}{\mathrm{d}z}[\mathbf{f}(z)] = \mathrm{i}\left[\underline{\underline{P}}\left(h\frac{\pi z}{\Omega}, \psi\right)\right]\cdot[\mathbf{f}(z)], \quad z > 0, \tag{7}$$

where the 4×4 matrix
and the scalar

$$\varepsilon_d = \frac{\varepsilon_a\varepsilon_b}{\varepsilon_a\cos^2\chi + \varepsilon_b\sin^2\chi}. \tag{9}$$

Equation (7) has to be solved numerically in order to determine the matrix $[\underline{\underline{Q}}]$ that appears in the relation

$$[\mathbf{f}(2\Omega)] = [\underline{\underline{Q}}]\cdot[\mathbf{f}(0+)] \tag{10}$$

to characterize the optical response of one period of the SCM.

By virtue of the Floquet theory [30], we can define a matrix $[\underline{\underline{\tilde{Q}}}]$ such that

$$[\underline{\underline{Q}}] = \exp\{\mathrm{i}2\Omega[\underline{\underline{\tilde{Q}}}]\}. \tag{11}$$

Both $[\underline{\underline{Q}}]$ and $[\underline{\underline{\tilde{Q}}}]$ share the same eigenvectors, and their eigenvalues are also related. Let $[\mathbf{t}]^{(n)}$, $(n = 1, 2, 3, 4)$, be the eigenvector corresponding to the nth eigenvalue σ_n of $[\underline{\underline{Q}}]$; then, the corresponding eigenvalue α_n of $[\underline{\underline{\tilde{Q}}}]$ is given by

$$\alpha_n = -\mathrm{i}\frac{\ln\sigma_n}{2\Omega}. \tag{12}$$

2.2. Dispersion equation

For the Dyakonov–Tamm wave to propagate parallel to $\hat{\mathbf{u}}_{\text{prop}}$, we must ensure that $\text{Im}(\alpha_{1,2}) > 0$, and set

$$[\mathbf{f}(0^+)] = [\,[\mathbf{t}]^{(1)} \quad [\mathbf{t}]^{(2)}\,] \cdot \begin{bmatrix} B_1 \\ B_2 \end{bmatrix}, \tag{13}$$

where B_1 and B_2 are unknown scalars, and $[\mathbf{f}(z^{\pm})]$ stands for $\lim_{\delta \to 0} [\mathbf{f}(z \pm \delta)]$ with $\delta \not< 0$. The other two eigenvalues of $[\underline{\underline{\tilde{Q}}}]$ describe waves that amplify as $z \to \infty$ and cannot therefore contribute to the Dyakonov–Tamm wave. At the same time

$$[\mathbf{f}(0^-)] = \begin{bmatrix} -\sin\psi & \frac{\alpha_{\text{TI}}}{k_0}\cos\psi \\ \cos\psi & \frac{\alpha_{\text{TI}}}{k_0}\sin\psi \\ \frac{\alpha_{\text{TI}}}{k_0}\eta_0^{-1}\cos\psi & n_{\text{TI}}^2\,\eta_0^{-1}\sin\psi \\ \frac{\alpha_{\text{TI}}}{k_0}\eta_0^{-1}\sin\psi & -n_{\text{TI}}^2\,\eta_0^{-1}\cos\psi \end{bmatrix} \cdot \begin{bmatrix} A_1 \\ A_2 \end{bmatrix}, \tag{14}$$

by virtue of equations (4) and (5).

Whereas the tangential component of the electric field phasor is continuous across the plane $z = 0$, the existence of the protected TISS on the boundary of the TI implies a discontinuity in the tangential component of the magnetic field phasor across the same plane [14, 20, 21]. Accordingly

$$\begin{bmatrix} 1 & 0 & 0 & 0 \\ 0 & 1 & 0 & 0 \\ -\gamma_{\text{TI}} & 0 & 1 & 0 \\ 0 & -\gamma_{\text{TI}} & 0 & 1 \end{bmatrix} \cdot [\mathbf{f}(0^-)] = [\mathbf{f}(0^+)], \tag{15}$$

which may be rearranged as

$$[\underline{\underline{M}}] \cdot \begin{bmatrix} A_1 \\ A_2 \\ B_1 \\ B_2 \end{bmatrix} = \begin{bmatrix} 0 \\ 0 \\ 0 \\ 0 \end{bmatrix}. \tag{16}$$

For a nontrivial solution, the 4×4 matrix $[\underline{\underline{M}}]$ must be singular, so that

$$\det\,[\underline{\underline{M}}] = 0 \tag{17}$$

is the dispersion equation for the Dyakonov–Tamm wave.

3. Numerical results and discussion

We numerically solved the dispersion equation to obtain the normalized wavenumbers $\tilde{q} = q/k_0$ of the Dyakonov–Tamm waves. Knowing q, we can calculate the phase speed $v_{\text{ph}} = c_0/\tilde{q}$ of the Dyakonov–Tamm wave. The spatial profile of the rate of energy flow associated with a Dyakonov–Tamm wave is provided via the time-averaged Poynting vector $\mathbf{P}(\mathbf{r}) \equiv \mathbf{P}(x, y, z) = (1/2)\text{Re}[\mathbf{e}(z) \times \mathbf{h}^*(z)]$, where the asterisk denotes the complex conjugate.

For all numerical results reported here, we fixed $\lambda_0 = 633$ nm and $\Omega = 197$ nm. For definiteness, the SCM

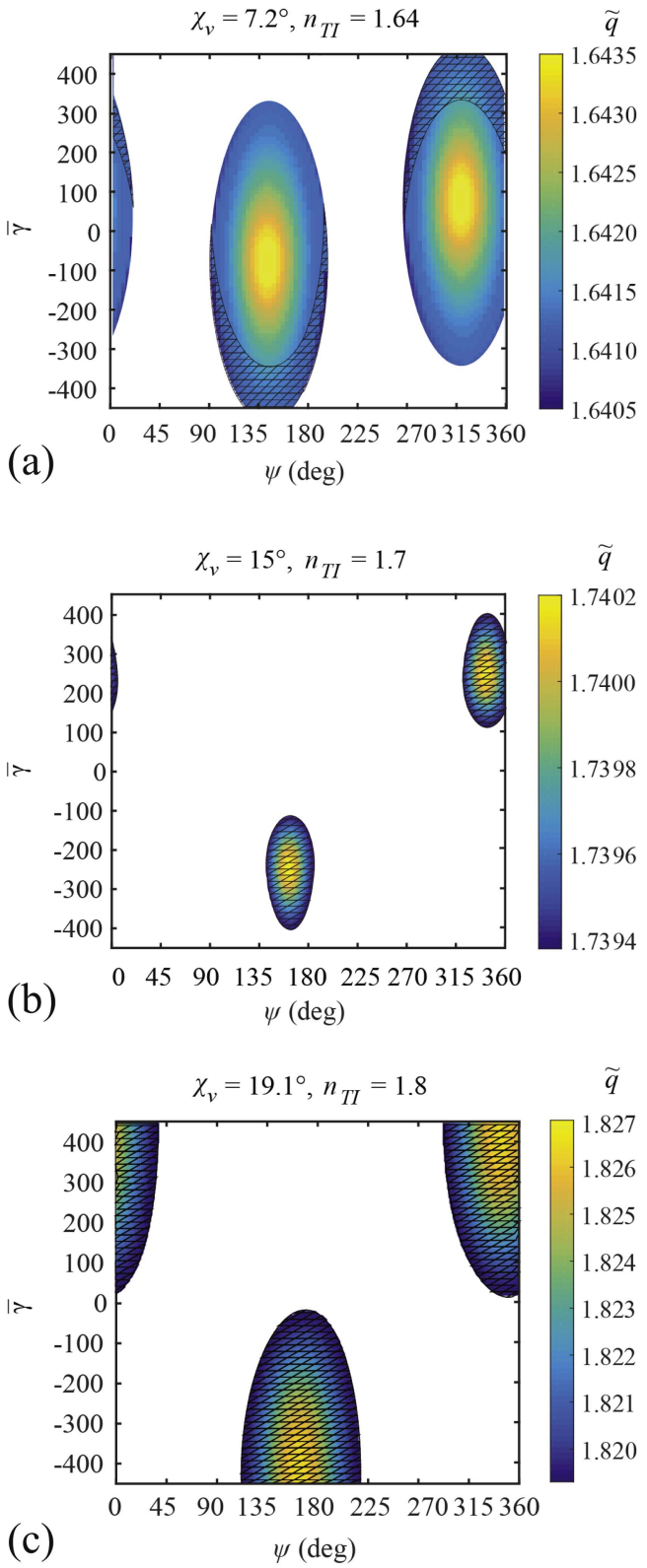

Figure 2. $\tilde{q}$ as a function of both ψ and $\bar{\gamma}$ for (a) $\chi_v = 7.2°$, $n_{\text{TI}} = 1.64$; (b) $\chi_v = 15°$, $n_{\text{TI}} = 1.7$; and (c) $\chi_v = 19.1°$, $n_{\text{TI}} = 1.8$. Cross hatching identifies those values of ψ for which a Dyakonov–Tamm wave exists but does not exist for $\psi \pm 180°$. Blank areas: no solution of equation (17).

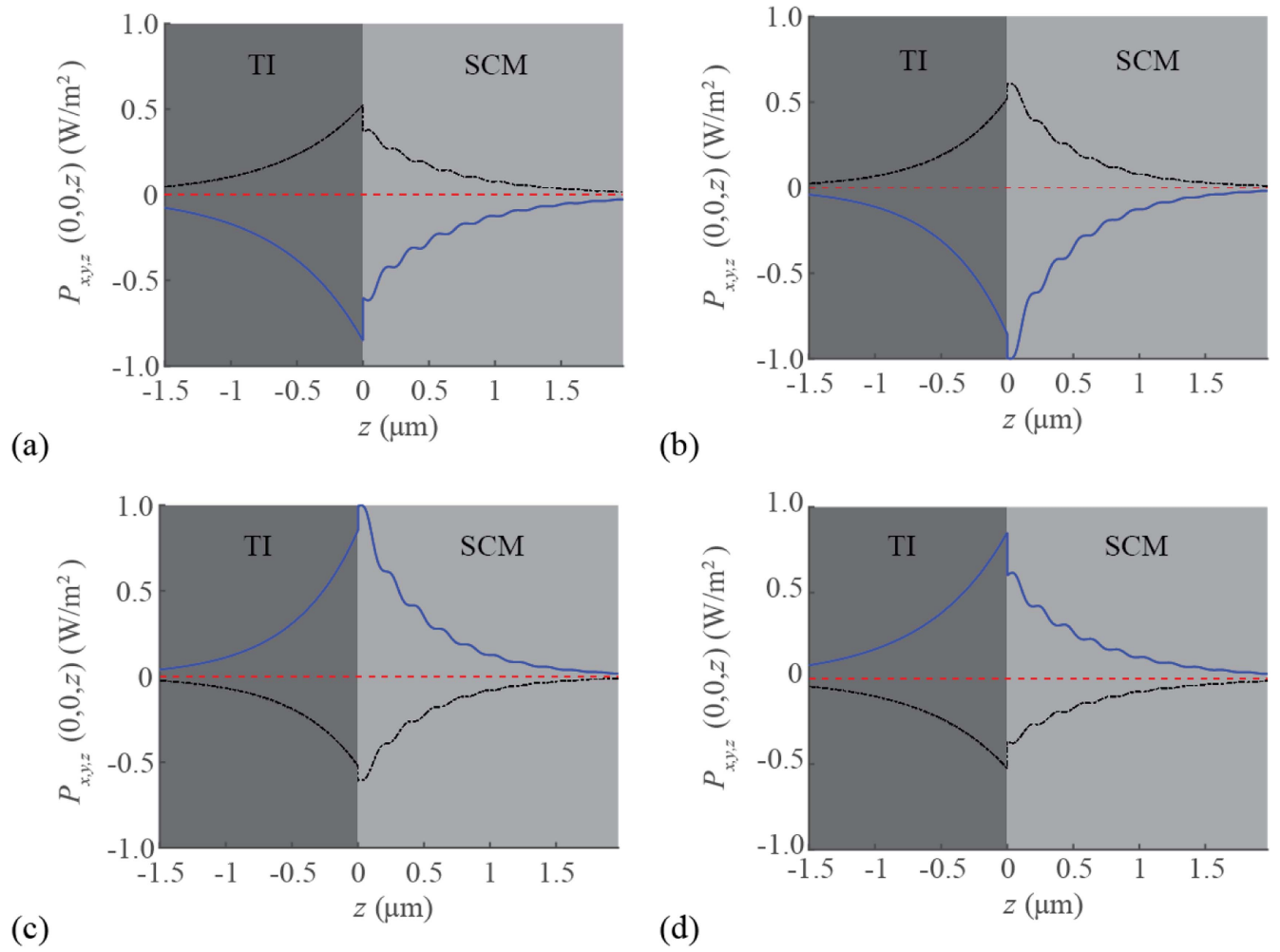

Figure 3. Spatial variations of the Cartesian components of the time-averaged Poynting vector $\mathbf{P}(0, 0, z)$ of the Dyakonov–Tamm wave guided by the TI/SCM interface when $\chi_v = 7.2°$ and $n_{\mathrm{TI}} = 1.64$. (a) $\psi = 148°$ and $\bar{\gamma} = 100$, (b) $\psi = 148°$ and $\bar{\gamma} = -100$, (c) $\psi = 328°$ and $\bar{\gamma} = 100$, (d) $\psi = 328°$ and $\bar{\gamma} = -100$. The components parallel to $\hat{\mathbf{u}}_x$, $\hat{\mathbf{u}}_y$, and $\hat{\mathbf{u}}_z$ are represented by blue solid, black broken dashed, and red dashed lines, respectively.

Table 1. Parameters in equation (20) delineating the regions in the $\psi\bar{\gamma}$ plane in which the propagation of Dyakonov–Tamm waves is allowed in figures 2(a)–(c).

Figure 2	χ_v	n_{TI}	ψ_C	ψ_D	$\bar{\gamma}_C$	$\bar{\gamma}_D$
(a)	7.2°	1.64	−38°	52°	80	450
(b)	15.0°	1.70	−18°	21°	248	145
(c)	19.1°	1.80	−16°	53°	415	395

was taken to be a chiral sculptured thin film, which comprises an array of parallel nanohelixes that rise at an angle χ to the interface plane by means of a vapor deposition process [23]. In accordance with empirical relationships determined for a columnar thin film of patinal titanium oxide produced by directing the vapor flux at an angle χ_v onto a rotating substrate, the principal relative permittivities are [31]

$$\left.\begin{aligned} \varepsilon_a &= \left[1.0443 + 2.7394\frac{\chi_v}{90} - 1.3697\left(\frac{\chi_v}{90}\right)^2\right]^2 \\ \varepsilon_b &= \left[1.6765 + 1.5649\frac{\chi_v}{90} - 0.7825\left(\frac{\chi_v}{90}\right)^2\right]^2 \\ \varepsilon_c &= \left[1.3586 + 2.1109\frac{\chi_v}{90} - 1.0554\left(\frac{\chi_v}{90}\right)^2\right]^2 \end{aligned}\right\} \quad (18)$$

with χ_v being in degree, and the angle

$$\chi = \arctan(2.8818 \tan \chi_v). \quad (19)$$

We considered $\chi_v = \{7.2°, 15.0°, 19.1°\}$ along with $n_{\mathrm{TI}} = \{1.64, 1.7, 1.8\}$, but kept $\bar{\gamma} = \eta_0 \gamma_{\mathrm{TI}} \tilde{\alpha}^{-1}$ variable, where $\tilde{\alpha} = 7.297352566 \times 10^{-3}$ is the fine structure constant [32]. The direction of propagation was also varied in the xy plane, i.e., $\psi \in [0°, 360°)$. All calculations were restricted to $n_{\mathrm{TI}} < \tilde{q} \leqslant 3$ to avoid computational instabilities that emerged

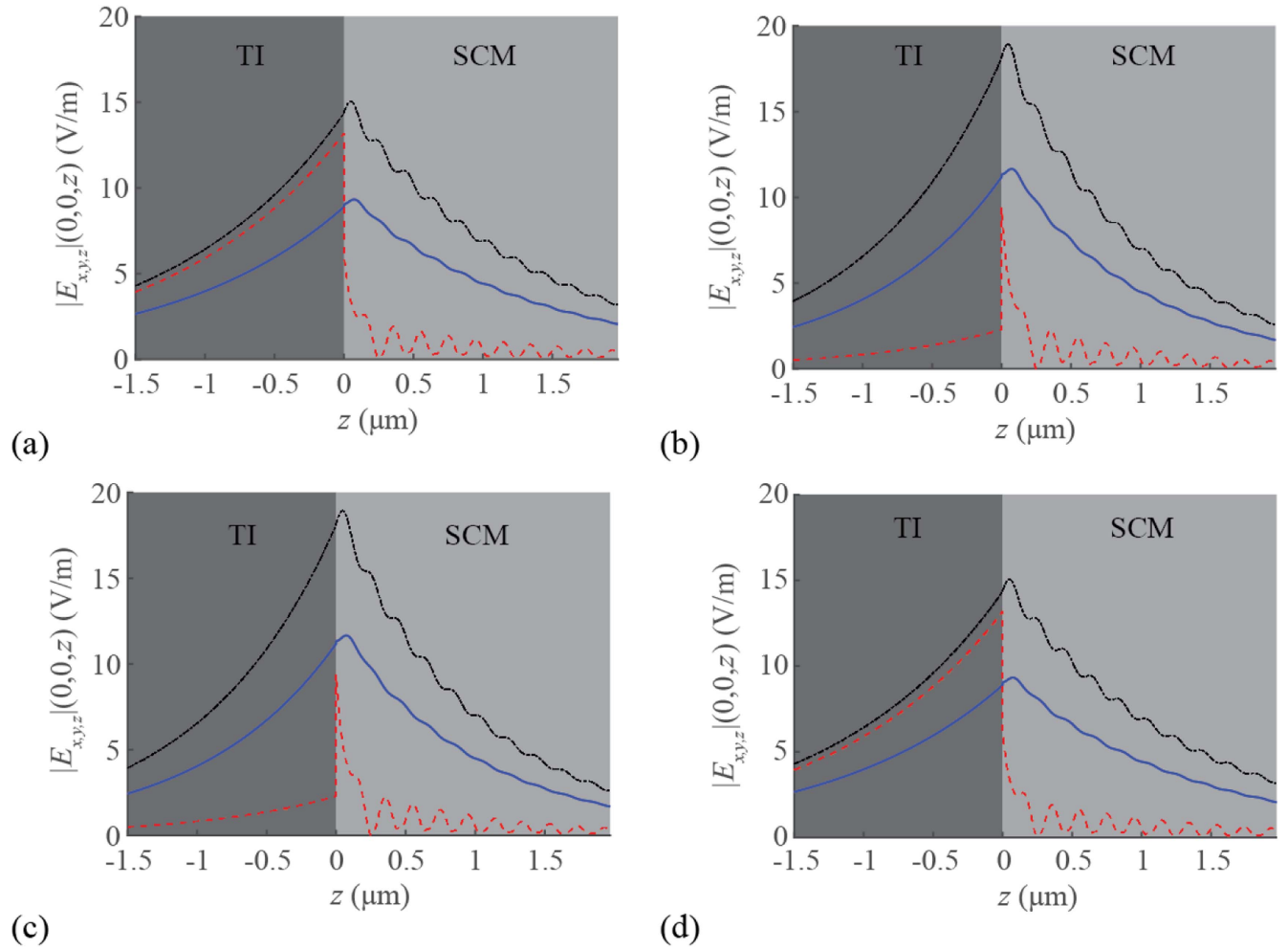

Figure 4. Same as figure 3 except that the magnitudes of the Cartesian components of the electric field phasor $\mathbf{E}(0, 0, z)$ are plotted.

for $\tilde{q} > 3$, whereas $\tilde{q}$ must be greater than n_{TI} to ensure that $\alpha_{\mathrm{TI}}^2 = k_0^2 n_{\mathrm{TI}}^2 - q^2 < 0$.

In figure 2(a), $\tilde{q}$ is displayed as a function of both ψ and $\bar{\gamma}$ when $\chi_v = 7.2°$ and $n_{\mathrm{TI}} = 1.64$. Solutions to the dispersion equation (17) were found in the range $1.6405 \leqslant \tilde{q} \leqslant 1.6435$ corresponding to a normalized phase speed v_{ph}/c_0 in the range $0.6085 \leqslant v_{\mathrm{ph}}/c_0 \leqslant 0.6096$. Dyakonov–Tamm-wave propagation is exhibited for $\psi \subseteq [0°, 16°] \cup [92°, 196°] \cup [272°, 360°]$, the widths of the angular sectors available for Dyakonov–Tamm-wave propagation being large in comparison to the $\lesssim 1°$ widths of angular sectors for Dyakonov-wave propagation [14].

The same is true in figure 2(b) for $\chi_v = 15°$ and $n_{\mathrm{TI}} = 1.7$, and in figure 2(c) for $\chi_v = 19.1°$ and $n_{\mathrm{TI}} = 1.8$. In figure 2(b), the solutions cover the range $1.7394 \leqslant \tilde{q} \leqslant 1.7402$, corresponding to normalized phase speeds in the range $0.5746 \leqslant v_{\mathrm{ph}}/c_0 \leqslant 0.5749$. In figure 2(c), the solutions cover the range $1.8193 \leqslant \tilde{q} \leqslant 1.8264$, corresponding to normalized phase speeds in the range $0.5475 \leqslant v_{\mathrm{ph}}/c_0 \leqslant 0.5497$.

All three panels in figure 2 indicate that the propagation of Dyakonov–Tamm waves, if it can occur for chosen values of the pair $\{\chi_v, n_{\mathrm{TI}}\}$, is possible in two non-overlapping regions in the $\psi\bar{\gamma}$ plane. Each region is bounded by an elliptical contour represented parametrically as the ellipse $\{\psi(\vartheta), \bar{\gamma}(\vartheta)\}$, with

$$\left.\begin{aligned} \psi(\vartheta) &= \psi_C + 180°\ell + \psi_D \cos\vartheta \,(\mathrm{mod}\ 360°) \\ \bar{\gamma}(\vartheta) &= (-1)^\ell \bar{\gamma}_C + \bar{\gamma}_D \sin\vartheta \end{aligned}\right\} \quad (20)$$
$$\vartheta \in [0°, 360°], \quad \ell \in \{1, 2\}.$$

The region described by $\ell = 1$ is located roughly in the center of the $\psi\bar{\gamma}$ plane in each panel, while the region described by $\ell = 2$ is split into two parts because $\psi(\vartheta)$ is cyclic with period 360°. The center of the ellipse is located at $\{\psi_C + 180°\ell, (-1)^\ell \bar{\gamma}_C\}$ for $\ell \in \{1, 2\}$, the projection of each ellipse on the ψ axis is $2\psi_D$, and the projection of each ellipse on the $\bar{\gamma}$ axis is $2\bar{\gamma}_D$. Values of the parameters $\psi_{C,D}$ and $\bar{\gamma}_{C,D}$ for all three panels are provided in table 1.

Figure 2 clearly shows that Dyakonov–Tamm waves are allowed for both positive and negative values of the surface admittance γ_{TI}. However, the angular sectors (on the ψ axis) are different for $\gamma_{\mathrm{TI}} > 0$ than for $\gamma_{\mathrm{TI}} < 0$.

Whereas Dyakonov–Tamm-wave propagation is possible for $\gamma_{\mathrm{TI}} = 0$ in figure 2(a), that is not true in figures 2(b) and (c). Therefore, the incorporation of the protected TISS with an

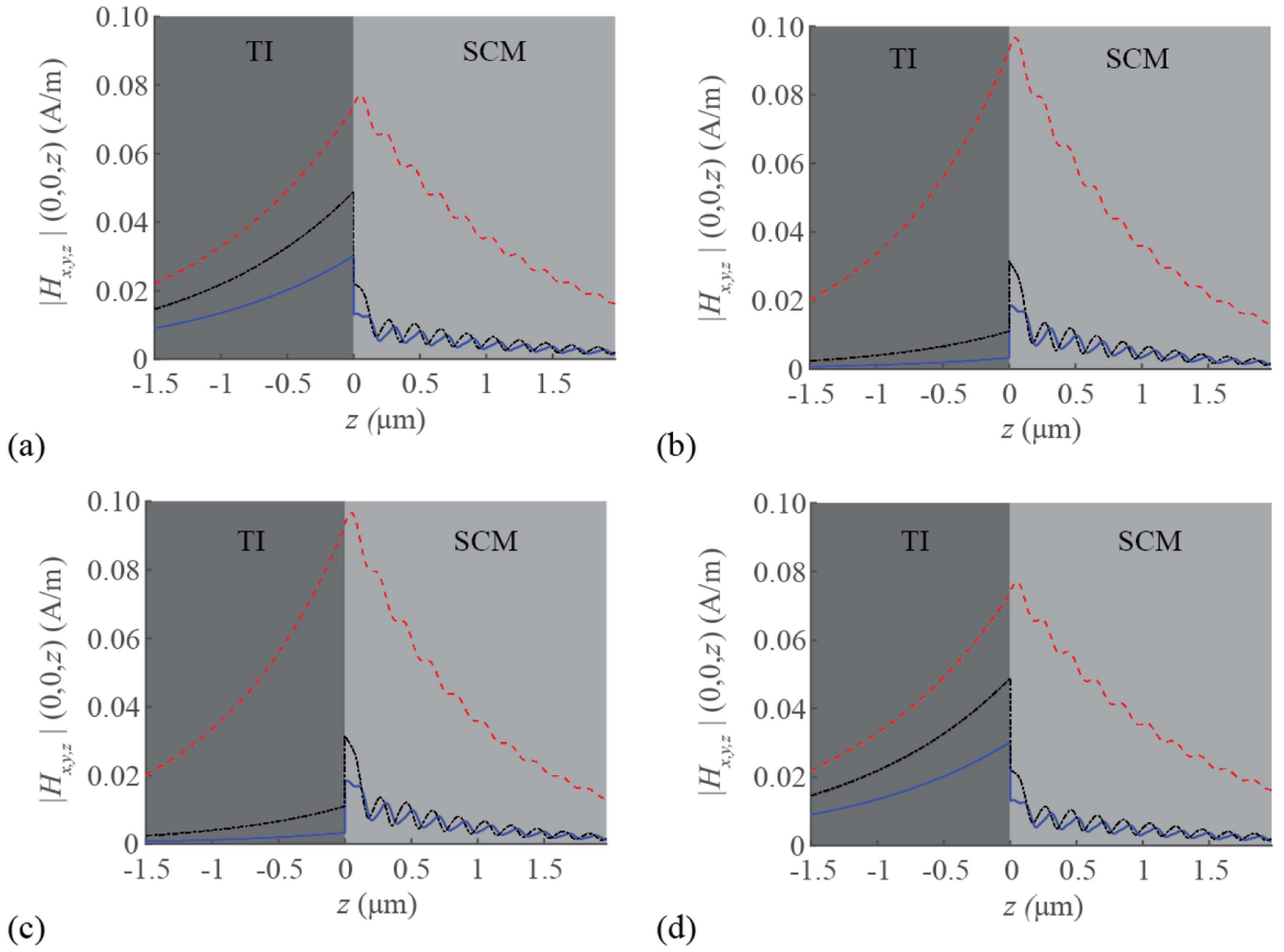

Figure 5. Same as figure 3 except that the magnitudes of the Cartesian components of the magnetic field phasor $\mathbf{H}(0, 0, z)$ are plotted.

appropriate value of γ_{TI} can trigger the excitation of Dyakonov–Tamm waves.

Left/right asymmetry is evident in all three panels in figure 2. If Dyakonov–Tamm waves are allowed to propagate in the two directions indicated by $\psi \in [0°, 180°]$ and $\psi + 180°$ for a specific value of $\gamma_{\mathrm{TI}} \neq 0$, the two Dyakonov–Tamm waves have different phase speeds (and, therefore, other characteristics). More significantly, figure 2 makes it clear that if a Dyakonov–Tamm wave can propagate in the direction indicated by $\psi \in [0°, 360°)$, there is also the likelihood that no Dyakonov–Tamm wave can propagate in the direction indicated by $\psi \pm 180°$. Cross hatching in all three panels highlights the values of ψ for which Dyakonov–Tamm-wave propagation is possible but not for $\psi \pm 180°$. These regions of *total* left/right asymmetry are very attractive for one-way devices, although they require high values of $|\bar{\gamma}|$ [17].

Further insights into the nature of these Dyakonov–Tamm waves may be gained by considering the spatial profiles of the Cartesian components of the electric and magnetic field phasors, along with those of the corresponding time-averaged Poynting vector. To allow for a consistent comparison, the amplitude of the time-averaged Poynting vector was constrained as $\hat{\mathbf{u}}_{\mathrm{prop}} \cdot \mathbf{P}(0, 0, 0^-) = 1\,\mathrm{W\,m^{-2}}$. Then, by virtue of equations (4) and (5), we get

$$|A_1|^2 = \frac{2\eta_0}{\tilde{q}} - \varepsilon_{\mathrm{TI}}|A_2|^2 \tag{21}$$

which allows all coefficients in the column vector on the left side of equation (16) to be specified.

The Cartesian components of $\mathbf{P}(0, 0, z)$ are plotted versus z in figure 3 for the Dyakonov–Tamm wave excited when $\chi_v = 7.2°$, $n_{\mathrm{TI}} = 1.64$, and $(\psi, \bar{\gamma}) \in \{(148°, \pm 100), (328°, \pm 100)\}$. A comparison of figures 3(a) and (b) reveals that, for $\psi = 148°$, the power density is slightly more confined to the TI when γ_{TI} is positive while for negative γ_{TI} the confinement is slightly greater to the SCM. In contrast, a comparison of figures 3(c) and (d) reveals that, for $\psi = 328°$, the power density is slightly more confined to the TI for negative γ_{TI} while the confinement is slightly greater to the SCM for positive γ_{TI}. After noting that $328° = 148° + 180°$, left/right asymmetry becomes evident on comparing figures 3(a) and (c) and/or comparing figures 3(b) and (d). The signs of P_x and P_y are reversed when together $\hat{\mathbf{u}}_{\mathrm{prop}}$ changes to $-\hat{\mathbf{u}}_{\mathrm{prop}}$ and γ_{TI} changes to $-\gamma_{\mathrm{TI}}$, as may be

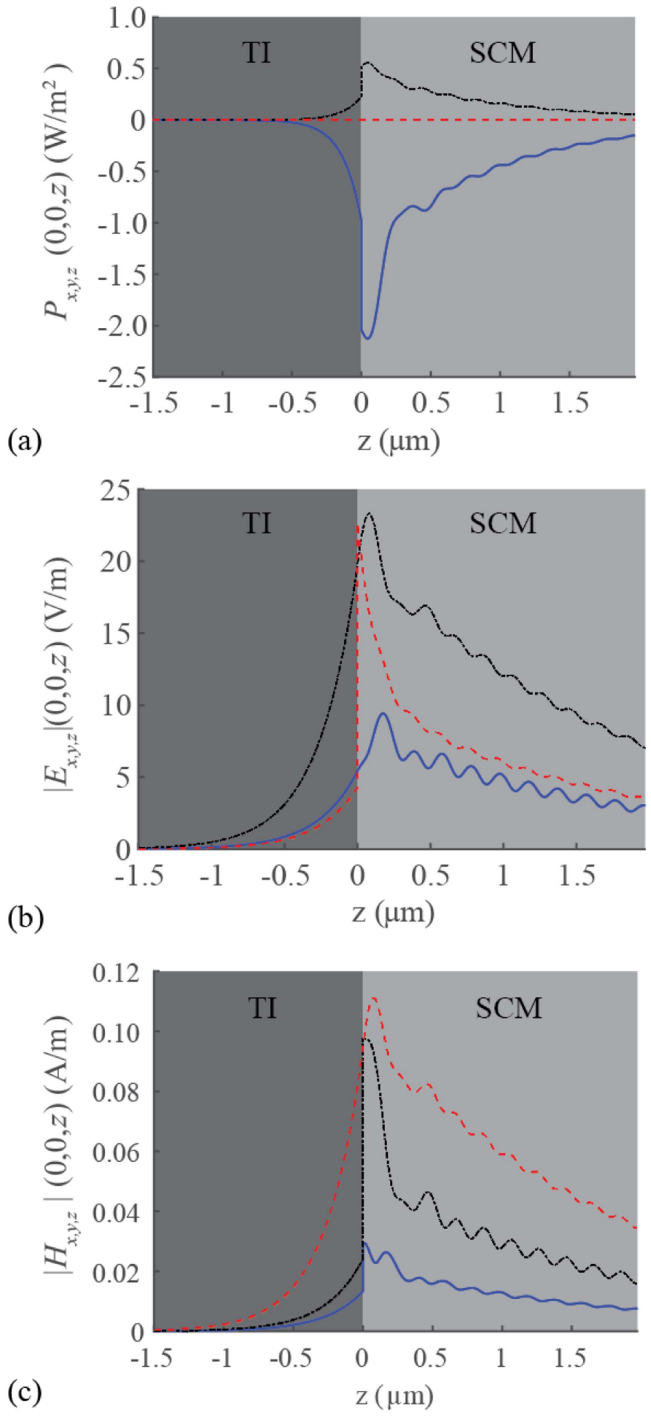

Figure 6. Spatial variations of the Cartesian components of (a) $\mathbf{P}(0, 0, z)$, (b) $\mathbf{E}(0, 0, z)$, and (c) $\mathbf{H}(0, 0, z)$ of the Dyakonov–Tamm wave guided by the TI/SCM interface when $\chi_v = 15°$, $n_{TI} = 1.70$, $\psi = 162°$, and $\bar{\gamma} = -248$. The components parallel to $\hat{\mathbf{u}}_x$, $\hat{\mathbf{u}}_y$, and $\hat{\mathbf{u}}_z$ are represented by blue solid, black broken dashed, and red dashed lines, respectively.

appreciated after comparing figures 3(b) and (c) and/or comparing figures 3(a) and (d).

Figures 4 and 5 show the magnitudes of the Cartesian components of $\mathbf{E}(0, 0, z)$ and $\mathbf{H}(0, 0, z)$ respectively, plotted against z for the same values of χ_v, n_{TI}, ψ, and $\bar{\gamma}$ as used for figure 3. All Cartesian components decay exponentially inside the TI as $z \to -\infty$, consistently with equations (4) and (5). The periodic undulations of the Cartesian components inside the SCM dampen as $z \to \infty$, in accord with the periodic nonhomogeneity of the SCM [27], as is warranted by Floquet theory [30].

The spatial profiles of the Cartesian components of the electric and magnetic field phasors in figures 4 and 5 vary relatively little in the SCM when either $\hat{\mathbf{u}}_{prop}$ changes to $-\hat{\mathbf{u}}_{prop}$ or γ_{TI} changes to $-\gamma_{TI}$, but more substantial variations are observed in the TI, especially for E_z, H_x, and H_y. Left/right asymmetry is obvious, e.g., on comparing figures 4(a) and (c) or comparing figures 5(b) and (d). Finally, the spatial profiles of the fields remain unchanged when $\hat{\mathbf{u}}_{prop}$ changes to $-\hat{\mathbf{u}}_{prop}$ and γ_{TI} changes to $-\gamma_{TI}$, as may be appreciated by comparing figures 4(b) and (c) and/or comparing figures 5(a) and (d).

Similar conclusions can be drawn looking at the spatial profiles for a case of total left/right asymmetry, in which Dyakonov–Tamm-wave propagation is possible for some ψ but not for $\psi \pm 180°$. As an example, figure 6 provides the spatial profiles of magnitudes of the Cartesian components of $\mathbf{P}(0, 0, z)$, $\mathbf{E}(0, 0, z)$, and $\mathbf{H}(0, 0, z)$ of the Dyakonov–Tamm wave guided by the TI/SCM interface when $\chi_v = 15°$, $n_{TI} = 1.70$, $\psi = 162°$, and $\bar{\gamma} = -248$. Dyakonov-wave propagation is not possible for $\psi = 342°$, other parameters remaining unchanged, according to figure 2(b). The spatial profiles in figure 6 are very similar to those in figures 3(b), 4(b), and 5(b), for which $\psi < 180°$ and $\bar{\gamma} < 0$.

A discussion of the discontinuities and continuities of the Cartesian components of the electric and magnetic field phasors across the plane $z = 0$ is in order. Both E_x and E_y must be continuous while E_z must be discontinuous, according to the standard boundary conditions of electromagnetics [33]. The plots in figures 4 and 6(b) are in accord with these constraints. As both partnering materials have been taken to be non-magnetic, H_z must be continuous across the plane $z = 0$ [33]. The plots in figures 5 and 6(c) show this continuity. The existence of the protected TISS must make H_x and H_y discontinuous across the plane $z = 0$, which is evident in figures 5 and 6(c). The continuities of E_x and E_y and the discontinuities of H_x and H_y were, of course, incorporated via equation (15).

4. Concluding remarks

We formulated and solved the boundary-value problem for electromagnetic surface waves guided by the planar interface of an SCM and a TI, both materials assumed to be non-magnetic. The protected TISS on the interface were quantitated through a surface admittance γ_{TI}. Our numerical investigation demonstrated that the phase speeds and the spatial profiles of Dyakonov–Tamm waves are significantly affected by γ_{TI}. A left/right asymmetry is exhibited whereby the phase speed and electromagnetic field profiles for a Dyakonov–Tamm wave that propagates co-parallel to a vector $\mathbf{u}$ in the interface plane are generally different to those for

a Dyakonov–Tamm wave that propagates anti-parallel to **u**. Even more importantly, the existence of a Dyakonov–Tamm wave that propagates co-parallel to a vector **u** in the interface plane does not imply the existence of a Dyakonov–Tamm wave that propagates anti-parallel to **u**. The left/right asymmetry, which vanishes if the surface admittance vanishes, is highly attractive for one-way on-chip optical communication.

Acknowledgments

TGM acknowledges the support of EPSRC Grant EP/M018075/1. A Lakhtakia thanks the Charles Godfrey Binder Endowment at the Pennsylvania State University for ongoing support of his research.

References

[1] Lakhtakia A and Polo J A Jr 2007 Dyakonov–Tamm wave at the planar interface of a chiral sculptured thin film and an isotropic dielectric material *J. Eur. Opt. Soc. Rapid Publ.* **2** 07021
[2] Yeh P, Yariv A and Hong C-S 1977 Electromagnetic propagation in periodic stratified media: I. General theory *J. Opt. Soc. Am.* **67** 423–38
[3] Yeh P, Yariv A and Cho A Y 1978 Optical surface waves in periodic layered media *Appl. Phys. Lett.* **32** 104–5
[4] Shinn M and Robertson W M 2005 Surface plasmon-like sensor based on surface electromagnetic waves in a photonic band-gap material *Sensors Actuators* B **105** 360–4
[5] Sinibaldi A, Danz N, Descrovi E, Munzert P, Schulz U, Sonntag F, Dominici L and Michelotti F 2012 Direct comparison of the performance of Bloch surface wave and surface plasmon polariton sensors *Sensors Actuators* B **174** 292–8
[6] Marchevskiĭ F N, Strizhevskiĭ V L and Strizhevskiĭ S V 1984 Singular electromagnetic waves in bounded anisotropic media *Sov. Phys. Solid State* **26** 911–2
[7] D'yakonov M I 1988 New type of electromagnetic wave propagating at an interface *Sov. Phys. JETP* **67** 714–6
[8] Takayama O, Crasovan L, Artigas D and Torner L 2009 Observation of Dyakonov surface waves *Phys. Rev. Lett* **102** 043903
[9] Pitarke J M, Silkin V M, Chulkov E V and Echenique P M 2007 Theory of surface plasmon and surface-plasmon polaritons *Rep. Prog. Phys.* **70** 1–87
[10] Jahani S and Jacob Z 2016 All-dielectric metamaterials *Nat. Nanotechnology* **11** 23–36
[11] Takayama O, Crasovan L-C, Johansen S K, Mihalache D, Artigas D and Torner L 2008 Dyakonov surface waves: a review *Electromagnetics* **28** 126–45
[12] Pulsifer D P, Faryad M and Lakhtakia A 2013 Observation of the Dyakonov–Tamm wave *Phys. Rev. Lett.* **111** 243902
[13] Pulsifer D P, Faryad M, Lakhtakia A, Hall A S and Liu L 2013 Experimental excitation of the Dyakonov–Tamm wave in the grating-coupled configuration *Opt. Lett.* **39** 2125–8
[14] Mackay T G and Lakhtakia A 2016 Nonreciprocal Dyakonov-wave propagation supported by topological insulators *J. Opt. Soc. Am.* B **33** 1266–70
[15] Chang M-C and Yang M-F 2009 Optical signature of topological insulators *Phys. Rev.* B **80** 113304
[16] Hasan M Z and Kane C L 2010 Topological insulators *Rev. Mod. Phys.* **82** 3045–67
[17] Maciejko J, Qi X-L, Drew H D and Zhang S-C 2010 Topological quantization in units of the fine structure constant *Phys. Rev. Lett.* **105** 166803
[18] Sayrin C, Junge C, Mitsch R, Albrecht B, O'Shea D, Schneeweiss P, Volz J and Rauschenbeutel A 2015 Nanophotonic optical isolator controlled by the internal state of cold atoms 2015 *Phys. Rev.* X **5** 041036
[19] Bohren C F and Hunt A J 1977 Scattering of electromagnetic waves by a charged sphere *Can. J. Phys.* **55** 1930–5
[20] Lakhtakia A and Mackay T G 2016 Electromagnetic scattering by homogeneous, isotropic, dielectric-magnetic sphere with topologically insulating surface states *J. Opt. Soc. Am.* B **33** 603–9
[21] Lakhtakia A and Mackay T G 2016 Classical electromagnetic model of surface states in topological insulators *J. Nanophoton.* **10** 033004
[22] de Gennes P G and Prost J A 1993 *The Physics of Liquid Crystals* 2nd edn (Oxford: Clarendon)
[23] Lakhtakia A and Messier R 2005 *Sculptured Thin Films: Nanoengineered Morphology and Optics* (Bellingham, WA: SPIE Press)
[24] Karch A 2011 Surface plasmons and topological insulators *Phys. Rev.* B **83** 245432
[25] Granada E J C and Rojas D F 2014 Local excitations in thin metal films bounded by topological insulators *Physica* B **455** 82–4
[26] Homola J (ed) 2006 *Surface Plasmon Resonance Based Sensors* (Berlin: Springer)
[27] Polo J A Jr, Mackay T G and Lakhtakia A 2013 *Electromagnetic Surface Waves: A Modern Perspective* (Waltham, MA: Elsevier)
[28] Pancharatnam S 1956 Generalized theory of interference and its applications *Proc. Indian Acad. Sci.* A **44** 247–62
[29] Berry M V 1984 Quantal phase factors accompanying adiabatic changes *Proc. R. Soc.* A **392** 45–57
[30] Yakubovich V A and Starzhinskii V M 1975 *Linear Differential equations with Periodic Coefficients* (New York: Wiley)
[31] Hodgkinson I, Wu Q H and Hazel J 1998 Empirical equations for the principal refractive indices and column angle of obliquely deposited films of tantalum oxide, titanium oxide, and zirconium oxide *Appl. Opt.* **37** 2653–9
[32] Bouchendira R, Cladé P, Guellati-Khélifa S, Nez F and Biraben F 2011 New determination of the fine structure constant and test of the quantum electrodynamics *Phys. Rev. Lett.* **106** 080801
[33] Iskander M F 2013 *Electromagnetic Fields and Waves* (Long Grove, IL: Waveland)